Sensitivity analysis of ozone formation and transport for a Central California air pollution episode

Ling Jin[1,2], *Shaheen Tonse*[2], *Daniel S. Cohan*[3], *Xiaoling Mao*[2], *Robert A. Harley*[4], *and Nancy J. Brown*[2*].

1. Energy and Resources Group, University of California, Berkeley, CA 94720

2. Atmospheric Sciences Department, Environmental Energy Technologies Division, Lawrence Berkeley National Laboratory, Berkeley, CA 94720

3. Dept. of Civil and Environmental Engineering, Rice Univ., Houston, TX 77005

4. Dept. of Civil and Environmental Engineering, University of California, Berkeley, CA 94720

* Corresponding author: njbrown@lbl.gov

Table of Contents brief

CMAQ-HDDM is used to determine spatial and temporal variations in ozone limiting reagents and local vs upwind source contributions for an air pollution episode in Central California.

Abstract

We developed a first- and second- order sensitivity analysis approach with the Decoupled Direct Method to examine spatial and temporal variations of ozone-limiting reagents and the importance of local vs upwind emission sources in the San Joaquin Valley of central California for a five-day ozone episode (29th July – 3rd Aug, 2000). Despite considerable spatial variations, nitrogen oxides (NO_x) emission reductions are overall more effective than volatile organic compound (VOC) control for attaining the 8-hr ozone standard in this region for this episode, in contrast to the VOC control that works better for attaining the prior 1-hr ozone standard. Inter-basin source contributions of NO_x emissions are limited to the northern part of the SJV, while anthropogenic VOC (AVOC) emissions, especially those emitted at night, influence ozone formation in the SJV further downwind. Among model input parameters studied here, uncertainties in emissions of NO_x and AVOC, and the rate coefficient of the OH+NO_2 termination reaction, have the greatest effect on first-order ozone responses to changes in NO_x emissions. Uncertainties in biogenic VOC emissions only have a modest effect because they are generally not collocated with anthropogenic sources in this region.

Introduction

The San Joaquin Valley (SJV) of California has serious ozone problems. Over the past decade, over 30 days/yr exceed the old 1-hr standard (120 ppb), and even more (>100 days/yr) exceed the 8-hr standard (84 ppb). Meeting the 8-hr standard is more difficult (1). Ozone is a secondary pollutant, and a key task in its control strategy design is to determine which precursor emissions to reduce: nitrogen oxides (NO_x) and/or volatile organic

compounds (VOC). The situation is complicated because ozone control regimes of NO_x-, and VOC-limitation, and transitional behavior change in both time and space as a function of emissions and meteorology (2-4). Consequently, understanding the spatial and temporal variations in ozone responses to anthropogenic emissions is important. The SJV is the recipient of both locally emitted and inter-basin transported pollutants (5), which further complicates the source receptor relationship and its policy implications. Quantification of the inter-basin transport contribution and its spatial extent is currently lacking.

Chemical transport models (CTMs) integrate scientific understanding of the key physical and chemical processes for ozone formation at regional or larger scales. Past studies for the SJV commonly used brute force methods conducted with CTMs to examine ozone responses to precursor pollutant changes by simulating scenarios with one-at-a-time perturbations of NO_x and/or VOC emissions (e.g. 6). Brute force methods become cumbersome as the number of emission scenarios increases. In contrast, the Decoupled Direct Method (DDM) efficiently calculates the local concentration derivatives to various parameters by separately solving sensitivity equations derived from the model equations (7-9), and has found wide applications in air quality models (e.g. 10,11,12). Because the accuracy of CTM simulations critically depends on the underlying input parameters, the influence of input uncertainties on ozone responses to emission reduction strategies needs to be assessed.

In this paper, we develop an analysis approach with High-order DDM (HDDM) within the Community Multiscale Air Quality (CMAQ) model (13) to investigate ozone sensitivities in the SJV during a high-ozone period with adverse meteorology that raises stringent demands for emissions control. We demonstrate this approach by exploring issues

important to ozone control in the SJV such as differences in control strategies in meeting the 1-hr and 8-hr ozone standards, changes in limiting reagent with time and space, importance of local vs upwind emission sources, and effects of emission timing. We assess the influences of uncertainties in emission inventories, reaction rate coefficients, and boundary conditions on the effects of anthropogenic emission reduction strategies with second-order sensitivity analyses.

Methods

Study domain and input data

The central California study domain is shown in Figure 1. The SJV is surrounded by Sierra Nevada and coastal mountain ranges. On typical summer days, westerly winds are funneled into the Central Valley through gaps in the coastal range with large portions of the flow directed into the SJV. The San Francisco Bay area (hereinafter Bay area) and Sacramento Valley are the major upwind emission sources affecting SJV air quality. The study domain is gridded into 96 by 117 cells, with a horizontal resolution of 4 km. Vertically, the domain is divided into 27 layers from the surface to 100 mb (about 17 km); the near surface layers are about 20 m thick.

We use emission inputs estimated for the period of Jul 29th to Aug 3rd in the summer 2000, similar to those of Steiner et al. (14), with additional fire emissions obtained from the California Air Resources Board. Hourly meteorological fields are simulated using the MM5 model by Wilczak and coworkers at NOAA (http://www.etl.noaa.gov/programs/modeling/ccos/) for a 15 day period from 24 Jul to 8 Aug 2000, with the middle 5 days characterized by stagnant conditions conducive to ozone formation and accumulation. Highest anthropogenic emissions are located near urban

centers and highway systems. Biogenic VOC emissions occur in vegetated regions, especially in the foothills of the Sierra Nevada and the coastal mountains. Soil NO_x emissions are not included in the inventory (see supporting information for uncertainty discussions). Emissions are summarized for the domain and sub-regions for weekdays and weekends, respectively in Table S1.

We performed extensive studies of model performance that are further described in the supporting information. Evaluation metrics (for 1-hr and 8-hr average peak ozone) reveal acceptable performance (Table S2 shows normalized bias within $\pm 15\%$, normalized gross error within $\pm 35\%$).

Constant pollutant concentrations are set for each of the domain's four lateral boundaries (Table S3). The western inflow boundary is mostly over the ocean and its chemical species are set to clean marine background concentrations. Vertically varying O_3 is based on averaged August ozone sonde measurements made at Trinidad Head, CA (15). Nitrogenous species (NO: 0.01 ppb; NO_2: 0.03 ppb; etc.) and a suite of VOC species take values measured in the marine background free troposphere (16). The other three boundaries are dominated by outflows; the same boundary values used in past studies conducted by the California Air Resources Board (17) are applied here. Influence of uncertainties in these boundary conditions on ozone responses to emission reductions are discussed later in the second-order sensitivity analysis.

CMAQ-HDDM modeling system

Since DDM equations follow the same structure as air quality model equations, their computational accuracy evolves with improvements in the CMAQ model. We have updated the existing implementation of HDDM (11) to work with the more recent CMAQ

version 4.5, which has a number of improvements to the chemistry, PBL modeling and the advection scheme. New features and improvements in this version of CMAQ-HDDM are summarized and evaluated in a paper by Napelenok et al. (18).

CMAQ-HDDM is configured with the piecewise parabolic method for advection, multiscale horizontal diffusion, eddy vertical diffusion, and the Euler Backward Iterative (EBI) ordinary differential equation solver. Gas phase chemistry is represented using the SAPRC99 chemical mechanism (19).

CMAQ-HDDM computes the first-order ($S_i^{(1)}$) and second-order ($S_{i,j}^{(2)}$) semi-normalized sensitivity coefficients.

$$S_i^{(1)} = P_i \frac{\partial C}{\partial p_i} = \frac{\partial C}{\partial \varepsilon_i} \tag{1}$$

$$S_{i,j}^{(2)} = P_i \frac{\partial}{\partial p_i}\left(P_j \frac{\partial C}{\partial p_j} \right) = \frac{\partial^2 C}{\partial \varepsilon_i \partial \varepsilon_j} \tag{2}$$

where, P_i is an input parameter, whose perturbation p_i is considered in a relative sense by defining a scaling variable ε_i with its nominal value being 1; $\boldsymbol{C}$ is the species concentration vector. Both first- and second-order sensitivity coefficients have concentration units. $S_i^{(1)}$ equaling α ppb implies that a $\pm 10\%$ change in the parameter would cause ($\pm 0.10\alpha$) ppb change in the ozone concentration while other parameters are held constant. $S_{i,j}^{(2)}$ is the sensitivity coefficient of a first-order sensitivity (Eq 2); it measures how a first-order sensitivity changes when another variable changes with respect to its nominal value, and

can be used to explore the non-linearities in a system. $S_{i,j}{}^{(2)}$ equaling α ppb implies that a $\pm 10\%$ change in the parameter *j* would cause ($\pm 0.10\alpha$) ppb change in $S_i{}^{(1)}$.

Ozone control regimes

First-order ozone sensitivities to domain-wide anthropogenic NO_x emissions ($\frac{\partial[O_3]}{\partial \varepsilon_{E_{NO_x}}}$) and to anthropogenic VOC (AVOC) emissions ($\frac{\partial[O_3]}{\partial \varepsilon_{E_{AVOC}}}$) are used to determine ozone-limiting reagents. Ozone responses to emission control options are represented using a first order approximation, which is likely to be valid for emission perturbations $\leq 25\%$ (20), which are usually suitable for policy applications.

We define three ozone control options, based on the relationship between the two sensitivity coefficients (see Fig. S1 for graphical illustration).

$\frac{\partial[O_3]}{\partial \varepsilon_{E_{NO_x}}} < 0$, VOC control,

$\frac{\partial[O_3]}{\partial \varepsilon_{E_{NO_x}}} > \frac{\partial[O_3]}{\partial \varepsilon_{E_{AVOC}}} > 0$, NO_x control,

$0 < \frac{\partial[O_3]}{\partial \varepsilon_{E_{NO_x}}} < \frac{\partial[O_3]}{\partial \varepsilon_{E_{AVOC}}}$, Transition.

The "VOC control" option is preferred when reducing AVOC reduces ozone concentration and reducing NO_x emissions would increase ozone concentrations (NO_x disbenefit). The "NO_x control" option is preferred when a percentage reduction in NO_x emissions results in larger decreases in ozone concentrations than the same percentage reduction in AVOC emissions. The third option is a transition regime, where reducing NO_x

emissions can reduce ozone concentrations, but is less effective than reducing AVOC by the same percentage.

Results and discussion

Simulated ozone and first-order sensitivity analysis

Surface ozone concentrations and first-order ozone sensitivity coefficients to domain-wide AVOC and NO_x emissions were calculated over a 5 day episode (Jul 29th – Aug 3rd), with a 3-day spin-up period for both simulations. Following spinup, the first two days are Sat-Sun, followed by three weekdays, which have similar AVOC but approximately 25% higher NO_x emissions due to changes in human activities (Table S1). Temperature increases over the episode, leading to 18% higher biogenic VOC (BVOC) emission rates during the later days of the simulation. Figure 2 presents simulation results averaged over the weekdays when the highest ozone levels occur. Color scales of dark orange and above in Figure 2ab indicate ozone exceedances. 1-hour exceedances in our domain are localized in the vicinity of high NOx and AVOC sources: downwind of the San Jose area and Livermore valley, downwind of Fresno, and downwind of Bakersfield (Figure 2a). In contrast, modeled 8-hour average ozone exceedances appear not only at locations that exceed the 1-hr standard, but also include rural areas in coastal ranges and Sierra foothills, which are further downwind of high emission centers (Figure 2b). In these high 8-hr ozone regions, $\frac{\partial[O_3]}{\partial \varepsilon_{E_{NO_x}}}$ changes signs (Figure 2d) and a NO_x disbenefit occurs in high NO_x areas: the Bay area and major urban centers. In contrast, $\frac{\partial[O_3]}{\partial \varepsilon_{E_{AVOC}}}$ is always positive, with higher

values collocated in NO_x rich areas ($\frac{\partial[O_3]}{\partial \varepsilon_{E_{NO_x}}} < 0$), indicating increasing AVOC reactivity with NO_x supply (Figure 2c).

A preference for AVOC control can be readily discerned for the Bay area from Figure 2bcd, because high ozone tends to be located in NO_x disbenefit areas. Further mapping of limiting reagents at the level of individual grid cells should be conducted to determine the most efficient control option in the SJV, especially for areas where both precursors have positive contributions to ozone formation.

Ozone control regimes in the SJV

Since areas with high 8-hr average ozone (> 84 ppb) in the SJV extend to suburban and rural areas (Figure 2 ab), there may be quite different limiting precursors for 8-hr vs 1-hr peak ozone. Even at the same location, the mean behavior captured by 8-hr averages can be quite different from individual hourly values.

Figure S1 indicates that control preferences for the 1-hour and 8-hour standards differ. Over 500 grid-hours of peak ozone in SJV exceed the 1-hr standard, and more than 50% of them indicate a preference for VOC control (Figure S1a), while NO_x control is preferred for only 14% of the grid-hours. Approximately 4000 grid-hours of the maximum 8-hr average ozone exceed the 8-hr standard. The majority (86%) of these 8-hr exceedances occurs at locations that did not exceed the 1-hr standard; more than 60% of the grid-hours indicate a preference for NO_x control whereas only 9% prefer VOC control (Figure S1c). Despite spatial variations, NO_x control is overall more beneficial for reducing 8-hr peak ozone in the SJV, in contrast to VOC control which works better for attaining the prior 1-hr standard.

Since preferred ozone control option regimes change in both time and space as a function of emissions and meteorology (2-4), we determined how ozone control options vary throughout the SJV and for different days in this episode. We determine daily ozone control options in the SJV at individual grid cells where 8-hr peak ozone exceeds the 8-hr standard, then map the results in Figure 3 according to the daily control options and whether they change across different days. Grid cells where the sign of ($\frac{\partial[O_3]}{\partial \varepsilon_{E_{NO_x}}}$) changes from day to day are colored gray. Weekends and weekdays are presented separately, for they differ in both emissions and meteorology during the simulation period. High ozone levels (> 84 ppb) are found along Highway 99 and Interstate 5 (marked in Fig 1) and areas downwind on both weekdays and weekends. The VOC control option is preferred for metropolitan areas in the SJV and places near Bay area and Sacramento emission sources for the weekdays (Figure 3a). NO_x control is preferred in the Sierra foothills and coastal ranges. Between urban and rural settings, where average $\frac{\partial[O_3]}{\partial \varepsilon_{E_{NO_x}}}$ is about to change sign (Figure 2c), ozone control options may change day by day (the grey areas in Figure 3), since NO_x control can be beneficial ($\frac{\partial[O_3]}{\partial \varepsilon_{E_{NO_x}}} > 0$) or detrimental (i.e. $\frac{\partial[O_3]}{\partial \varepsilon_{E_{NO_x}}} < 0$) at the same location on different days. Since weekday emissions are modeled to be almost identical, these changes are most likely caused by day-to-day differences in meteorology. Temperatures on the weekends are 3-5 degrees (K) cooler, resulting less extensive ozone exceedances as seen in Figure 3b. Compared to the weekday sensitivity map, ozone control on weekends in this episode would be better served by NO_x control, including a number of rural areas that were in "NO_x transition" on weekdays. This is partly due to greater ozone sensitivities to NO_x emissions when NO_x levels are lower on weekends, which is referred

to as a concave daytime ozone response to NO_x emissions (21). Our findings agree with studies by Reynolds et al (1) that were conducted for the same domain but a different ozone episode (see Supporting Information).

Local vs upwind source contributions

Typically, emissions over the whole modeling domain are perturbed for calculating ozone sensitivities, so that all possible anthropogenic emissions that may influence air quality are included. Consequently, the ozone control option derived from these sensitivities is a "regional decision". In reality, air quality is usually managed at air basin scales. The first-order ozone sensitivity to domain-wide emissions for any location is equal to the sum of ozone sensitivities to emissions associated with each air basin, or even further divided sub-regions. These various sensitivities may vary greatly in magnitude and sign. A study objective is to develop an analysis approach that could be used to determine the relative importance of intra- and inter-basin transport. Understanding contributions from each sub-region is particularly important for the SJV because it is downwind of large emission sources, and their role in SJV air pollution is not understood. It is not clear whether the "regional decision" should be applied to SJV alone or whether upwind air basins should be included in order to achieve effective ozone control.

Ozone sensitivity to Bay area emissions is used to illustrate the importance of inter-basin contributions. Ozone sensitivities to emissions from the northern, middle, and southern SJV (Figure 1) are calculated so that local and intra-basin contributions can be further distinguished. For example, at locations in the southern SJV, ozone sensitivities to southern SJV emissions represent the local contribution, while ozone sensitivities to emissions from other parts of the SJV represent intra-basin contributions. Local, intra-basin, and inter-basin

source contributions to the peak 8-hr ozone levels at grid cells along two transects (black dash-dotted lines in Figure 3) are averaged over the weekdays and presented in Figure 4 The western transect is along the I-5 transportation corridor, which runs through rural areas and passes locations that are out of compliance with the 8-hr standard. The eastern transect is along Highway 99, which runs through major SJV metropolitan areas and their downwind areas, where 8-hour ozone exceedances also occur. Both transects start from Tracy (indicated in Figure 3) in the northern SJV and move downwind away from the Bay area toward the southern SJV. The sub-regional contributions considered here do not add up to ozone sensitivity to domain wide emissions (the black dotted line, hereinafter called "regional contribution"), because emissions from other air basins also play a role.

Along the eastern transect, ozone responses to changes in domain wide emissions are largely determined by local contributions, with only a few exceptions (Figure 4ab): emissions from the Bay area determine ozone sensitivities at locations near Tracy in the northern SJV; AVOC contributions from the Bay area and other parts of the SJV account for more than 50% of the ozone responses in the southern SJV as it is downwind of all the other emission sources. Sign difference between regional and local contributions occurs at a few places especially between urban emission sources (Figure 4a). For example, upon entering the southern SJV, positive contributions of NO_x emissions from the middle SJV and further upwind areas dominate the local NO_x disbenefit, so that ozone sensitivity to domain-wide NO_x emissions is positive. At places like this, when regional NO_x control is applied locally, it must be accompanied by NO_x controls in upwind areas to achieve ozone reductions. The general trend for sensitivity to NO_x is that local controls exhibit a NO_x disbenefit, but reduce ozone formation as air masses are transported downwind. Inter-basin

contributions due to NO_x emissions from the Bay area are only important for the northern SJV. In contrast, positive and significant $\frac{\partial[O_3]}{\partial \varepsilon_{E_{SFBAVOC}}}$ indicate that Bay area AVOC emissions influence ozone formation in the northern and the middle SJV.

Along the western transect, the influence of Bay area emissions reaches further downwind for the ozone episode considered here (Figure 4cd). Bay area NO_x emissions largely determine the sign and magnitude of regional contributions to ozone responses in the northern SJV, while in the middle and southern SJV, local and intra-basin contributions are more important. A positive and significant influence of Bay area AVOC emissions dominates ozone formation along the western transect. Therefore, the VOC control option preferred in the Bay area not only benefits local air quality, but also reduces downwind ozone significantly. Along both transects, NO_x emitted in the Bay area has a shorter lifetime for influencing SJV ozone formation than Bay area AVOC emissions.

Bay area AVOC emissions contribute to SJV ozone concentrations by: (1) being transported to the SJV, thus increasing the SJV local precursor budget; and (2) forming ozone en route, thereby directly increasing SJV ozone levels by transport. In both cases, emission timing is important for inter-basin transport of pollutants because photochemical production of ozone occurs during the day. Bay area AVOC emissions were perturbed in three different time intervals: morning (5 AM to noon), afternoon (noon to 7 PM), and evening (7 PM to next day 5 AM). Relative contributions to the increase of VOC and ozone concentrations due to Bay area AVOC emissions were calculated, and averaged over 8-hr peak ozone peak period at Tracy in the northern SJV and Fresno in the middle SJV (Figure S2). Although the VOC concentrations in the northern SJV are most sensitive to

Bay area afternoon emissions (~55% of $\frac{\partial[VOC]}{\partial \varepsilon_{E_{SFBAVOC}}}$), ozone levels are most sensitive to Bay area morning emissions (~50% of $\frac{\partial[O_3]}{\partial \varepsilon_{E_{SFBAVOC}}}$). The most reactive AVOC emissions from the Bay area are consumed before reaching Tracy, but the resulting odd oxygen (O_3+NO_2) that is formed contributes to ozone levels by transport. In contrast to Tracy, Fresno is further downwind from the Bay area, and at Fresno, both VOC and ozone are most sensitive to Bay area evening emissions (70%) from the previous day. Bay Area evening VOC emissions are transported further downwind in air masses that are not photochemically active. Air masses containing Bay area evening VOC emissions pass by Tracy, and arrive at Fresno when the sun rises so they can actively participate in daytime ozone production. Evening emissions contribute about the same percentage increase to VOC and ozone concentrations, which indicates they increase ozone concentrations in the middle SJV by increasing downwind VOC budget (Figure S2).

In contrast to the conceptual model proposed by Pun et al (5) (see supporting information), we have developed a quantitative method to assess the importance of inter- and intra- basin transport on ozone formation and its accumulation across both urban and rural settings. In the 5-day episode considered here, we found differentiated contributions from Bay area NO_x and AVOC emissions to the air quality in the SJV. Bay area AVOC emissions, especially those emitted at night, influence ozone levels in the SJV further downwind, while NO_x emissions mainly affect the northern part of the SJV. Two things should be noted for this analysis. First, the relative and absolute inter-basin contributions reported here are only representative of the meteorological conditions in this particular ozone episode when westerly flow is weak (Supporting Information). Second, the

importance of inter-basin and intra-basin emissions is compared based on source contributions (same percentage perturbations in emission sources), into which the regional contribution ($\frac{\partial[O_3]}{\partial \varepsilon_{E_{AVOC}}}$ or $\frac{\partial[O_3]}{\partial \varepsilon_{E_{NOx}}}$) can be decomposed. Since Bay area emissions are about three times those from each of three parts of the SJV (Table S1), if ozone sensitivities to absolute mass emissions are considered, influences of Bay area emissions on the SJV ozone levels would be less pronounced in the middle and southern SJV.

Influence of uncertainties in other parameters

Findings with first-order sensitivity coefficients are applicable to small emission reductions for a given set of model inputs and parameters. Second-order sensitivities measure the sensitivity of first-order sensitivities to other input variable changes, and are used here to quantify how ozone responses to NO_x emissions are influenced by other model uncertainties (21). We consider how $\frac{\partial[O_3]}{\partial \varepsilon_{E_{NO_x}}}$ changes with uncertainties in other model inputs because our results indicate that NO_x control is preferred for abating 8-hr peak ozone in the SJV. Also, Hakami et al. (11) found that changes in NO_x emissions in Central California produced the most non-linear ozone response. Six model input parameters were selected for the second order sensitivity of $\frac{\partial[O_3]}{\partial \varepsilon_{E_{NO_x}}}$: NO_x emissions, AVOC emissions, rate coefficient of the $OH+NO_2$ reaction, BVOC emissions, O_3 inflow boundary conditions, and NO_y inflow boundary conditions. Large second order sensitivities usually appear when both first-order sensitivities are large (20,22). Hence, the selection of the second variable is based on relatively large first-order sensitivity as well as high uncertainty. All second

order sensitivity coefficients are semi-normalized as indicated in Eq. (2) to facilitate comparison.

Weekday second-order sensitivity maps are shown in Figure 5; the sensitivities are averaged over the peak 8-hr ozone hours, and are shown in order of decreasing magnitude. $\frac{\partial}{\partial \varepsilon_{E_{NO_x}}}\left(\frac{\partial [O_3]}{\partial \varepsilon_{E_{NO_x}}}\right)$ has the largest magnitude, and is negative over most of the domain, except part of the Bay area with low ozone concentrations (Figure 5a and Figure 2ab). There are abrupt changes in the sign of second-order sensitivities in Figures 5a,b, and d. This is due to a transition from a region where NO_x titrates ozone to one where more photochemical ozone production occurs.

$\frac{\partial}{\partial \varepsilon_{E_{AVOC}}}\left(\frac{\partial [O_3]}{\partial \varepsilon_{E_{NO_x}}}\right)$ is mostly positive except in part of the Bay area with low ozone concentrations, and it is large where $\frac{\partial}{\partial \varepsilon_{E_{NO_x}}}\left(\frac{\partial [O_3]}{\partial \varepsilon_{E_{NO_x}}}\right)$ is large but of the opposite sign. The magnitudes of $\frac{\partial}{\partial \varepsilon_{E_{NO_x}}}\left(\frac{\partial [O_3]}{\partial \varepsilon_{E_{NO_x}}}\right)$ and $\frac{\partial}{\partial \varepsilon_{E_{AVOC}}}\left(\frac{\partial [O_3]}{\partial \varepsilon_{E_{NO_x}}}\right)$ tend to reach their maxima at places where $\frac{\partial [O_3]}{\partial \varepsilon_{E_{NO_x}}}$ is about to change signs (Figure S3), corresponding to the grey areas between urban and rural settings in Figure 3a. Therefore, not only are control options in these grey areas more sensitive to meteorological variations than typical urban or rural areas as found earlier, but also their accuracy is more susceptible to emission uncertainties. The $OH+NO_2$ chain terminating reaction, which removes HO_x and NO_x from the air mass, is one of the most important reactions in determining ozone production (23). This rate coefficient is the third most influential variable for ozone responses to NO_x emissions and the sensitivity of

$\frac{\partial[O_3]}{\partial \varepsilon_{E_{NO_x}}}$ to it is mostly positive throughout the SJV, where increasing it would make ozone sensitivity to the remaining NO_x more positive. If this rate coefficient was increased, ozone levels would be more responsive to NO_x emissions at locations downwind of Bakersfield (see Fig S3). BVOC emissions are the largest VOC source in the domain; however, their influence on $\frac{\partial[O_3]}{\partial \varepsilon_{E_{NO_x}}}$ is much less than AVOC. Since cross derivatives of two pollutant emission sources increase with their proximity to each other (21), and BVOC is generally not collocated with high NO_x emissions, its influence is greatly reduced. Nevertheless, doubling BVOC emissions inputs would increase ozone sensitivities to NO_x emissions by 10 ppb in certain places (e.g. downwind of Fresno, see Fig S3), and thus increase the responsiveness to NO_x control. Our assumption of constant boundary conditions introduces uncertainties to the modeling system as boundary conditions vary by season and are influenced by inter-continental transport of pollution (16). Uncertainties in boundary ozone could change ozone response to NO_x emissions by about 5 ppb, whereas the influence from specification of boundary NO_y concentrations is negligible, assuming a clean marine air mass as inflow (Figure S4).

Acknowledgement

Support for this study was provided by the California Energy Commission, the California Air Resources Board, the UC Toxic Substances Research and Teaching Program student fellowship, and by the Assistant Secretary for Fossil Energy, Office of Natural Gas and Petroleum Technology through the National Petroleum Technology Office under U.S. Department of Energy Contract No. DE-AC03-76SF00098. The authors thank James

Wilczak, Jian-Wen Bao, and Sara Michelson for providing MM5 meteorological fields, and Allison Steiner for providing the biogenic emission inventory used in this research.

Supporting Information Available

Summary table of emission inputs (Table S1), model evaluation metrics (Table S2), description of meteorological and emission inputs, contrast to previous studies, boundary conditions for selected species (Table S3), scatter plots of ozone control options for 1-hr and 8-hr peak ozone exceedances in the SJV (Figure S1), contributions from Bay area emissions at different time intervals (Figure S2), and second order sensitivity coefficients along two transects (Figure S3), and for the whole domain (Figure S4) are available free of charge via the Internet at http://pubs.acs.org.

Literature Cited

(1) Reynolds, S. D.; Blanchard, C. L.; Ziman, S. D. Understanding the effectiveness of precursor reductions in lowering 8-Hr ozone concentrations. *Journal of the Air & Waste Management Association* **2003**, *53*, 195-205.

(2) Blanchard, C. L.; Stoeckenius, T. Ozone response to precursor controls: comparison of data analysis methods with the predictions of photochemical air quality simulation models. *Atmospheric Environment* **2001**, *35*, 1203-1215.

(3) Baertsch-Ritter, N.; Keller, J.; Dommen, J.; Prevot, A. S. H. Effects of various meteorological conditions and spatial emission resolutions on the ozone concentration and ROG/NOx limitation in the Milan area (I). *Atmospheric Chemistry And Physics* **2004**, *4*, 423-438.

(4) Couach, O.; Kirchner, F.; Jimenez, R.; Balin, I.; Perego, S.; van den Bergh, H. A development of ozone abatement strategies for the Grenoble area using modeling and indicators. *Atmospheric Environment* **2004**, *38*, 1425-1436.

(5) Pun, B. K.; Louis, J. F.; Pai, P.; Seigneur, C.; Altshuler, S.; Franco, G. Ozone formation in California's San Joaquin Valley: A critical assessment of modeling and data needs. *Journal Of The Air & Waste Management Association* **2000**, *50*, 961-971.

(6) Dabdub, D.; DeHaan, L. L.; Seinfeld, J. H. Analysis of ozone in the San Joaquin Valley of California. *Atmospheric Environment* **1999**, *33*, 2501-2514.

(7) Dunker, A. M. Efficient Calculation Of Sensitivity Coefficients For Complex Atmospheric Models. *Atmospheric Environment* **1981**, *15*, 1155-1161.

(8) Yang, Y. J.; Wilkinson, J. G.; Russell, A. G. Fast, Direct Sensitivity Analysis of Multidimensional Photochemical Models. *Environ. Sci. Technol.* **1997**, *31*, 2859-2868.

(9) Dunker, A. M.; Yarwood, G.; Ortmann, J. P.; Wilson, G. M. The decoupled direct method for sensitivity analysis in a three-dimensional air quality model - Implementation, accuracy, and efficiency. *Environmental Science & Technology* **2002**, *36*, 2965-2976.

(10) Hakami, A.; Odman, M. T.; Russell, A. G. High-order, direct sensitivity analysis of multidimensional air quality models. *Environmental Science & Technology* **2003**, *37*, 2442-2452.

(11) Hakami, A.; Odman, M. T.; Russell, A. G. Nonlinearity in atmospheric response: A direct sensitivity analysis approach. *Journal Of Geophysical Research-Atmospheres* **2004**, *109*, D15303, doi: 10.1029/2003JD004502

(12) Napelenok, S. L.; Cohan, D. S.; Hu, Y.; Russell, A. G. Decoupled direct 3D sensitivity analysis for particulate matter (DDM-3D/PM). *Atmospheric Environment* **2006**, *40*, 6112-6121.

(13) Byun, D. W.; Schere, K. L. Review of the governing equations, computational algorithms, and other components of the Models-3 Community Multiscale Air Quality (CMAQ) modeling system. *Applied Mechanics Reviews* **2006**, *59*, 51-77.

(14) Steiner, A. L., S. Tonse, R. C. Cohen, A. H. Goldstein, R. A. Harley Influence of future climate and emissions on regional air quality in California. *J. Geophys. Res.* **2006**, *111*, D18303, doi: 10.11029/12005JD006935.

(15) Newchurch, M. J.; Ayoub, M. A.; Oltmans, S.; Johnson, B.; Schmidlin, F. J. Vertical distribution of ozone at four sites in the United States. *Journal Of Geophysical Research-Atmospheres* **2003**, *108*, D14031, doi:10.1029/2002JD002059
.

(16) Nowak, J. B., D. D. Parrish, J. A. Neuman, J. S. Holloway, O. R. Cooper, T. B. Ryerson, J. D.K. Nicks, F. Flocke, J. M. Roberts, E. Atlas, J. A. d. Gouw, S. Donnelly, E. Dunlea, G. H, L. G. Huey, S. Schauffler, D. T. Sueper, D. J. Tanner, C. Warneke, F. C. Fehsenfeld, Gas-phase chemical characteristics of Asian emission plumes observed during ITCT 2K2 over the eastern North Pacific Ocean. *J. Geophys. Res.* **2004**, *109*, D23S19, doi:10.1029/2003JD004488.

(17) Kaduwela, A., California Air Resources Board, Sacramento, CA, personal communication, 2006.

(18) Napelenok, S. L.; Cohan, D. S.; Odman, M. T.; Tonse, S. Extension and evaluation of sensitivity analysis capabilities in a photochemical model., Submitted to Environmental Modeling & Software, currently under review, 2007.

(19) Carter, W. P. L. Implementation of the SARPRC-99 Chemical Mechanism into the Model-3 Framework. University of California, Riverside, California, Report to the U.S. Environmental Protection Agency. 2000.

(20) Vuilleumier, L.; Harley, R. A.; Brown, N. J. First- and second-order sensitivity analysis of a photochemically reactive system (a Green's function approach). *Environmental Science & Technology* **1997**, *31*, 1206-1217.

(21) Cohan, D. S.; Hakami, A.; Hu, Y. T.; Russell, A. G. Nonlinear response of ozone to emissions: Source apportionment and sensitivity analysis. *Environmental Science & Technology* **2005**, *39*, 6739-6748.

(22) Brown, N. J.; Revzan, K. L. Comparative sensitivity analysis of transport properties and reaction rate coefficients. *International Journal Of Chemical Kinetics* **2005**, *37*, 538-553.

(23) Martien, P. T.; Harley, R. A. Adjoint sensitivity analysis for a three-dimensional photochemical model: Application to Southern California. *Environmental Science & Technology* **2006**, *40*, 4200-4210.

Figures

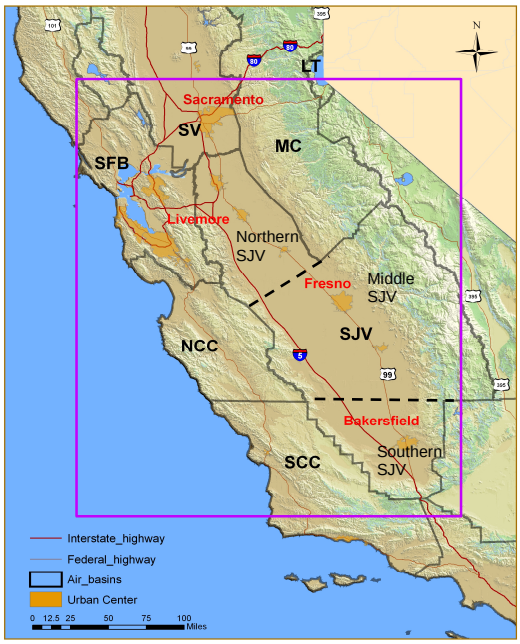

Figure 1. Modeling domain indicated by the purple rectangle. Air basins are labeled on the map for San Francisco Bay Area (SFB), Sacramento Valley (SV), Mountain County (MC), San Joaquin Valley (SJV), North and South Central Coast (NCC and SCC).

SJV is further divided into three parts (Northern, Middle, and Southern part) as indicated by dashed lines.

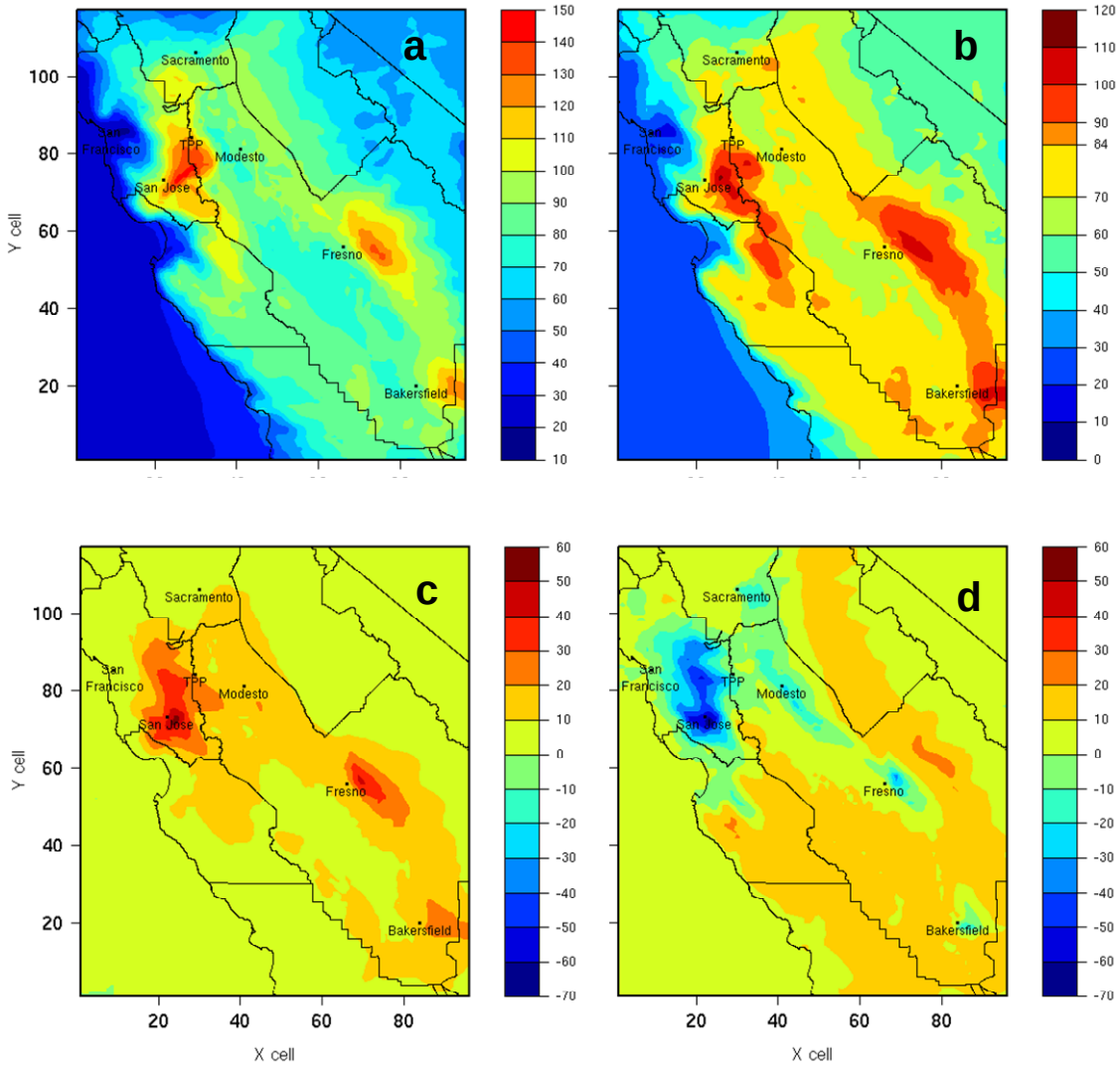

Figure 2. Weekday average simulation results (in ppb): **a**. 1-hr peak ozone concentrations, **b**. 8-hr average peak ozone concentrations, **c**. 8-hr average peak ozone sensitivity to domain wide AVOC emissions, **d**. 8-hr average peak ozone sensitivity to domain wide anthropogenic NO_x emissions.

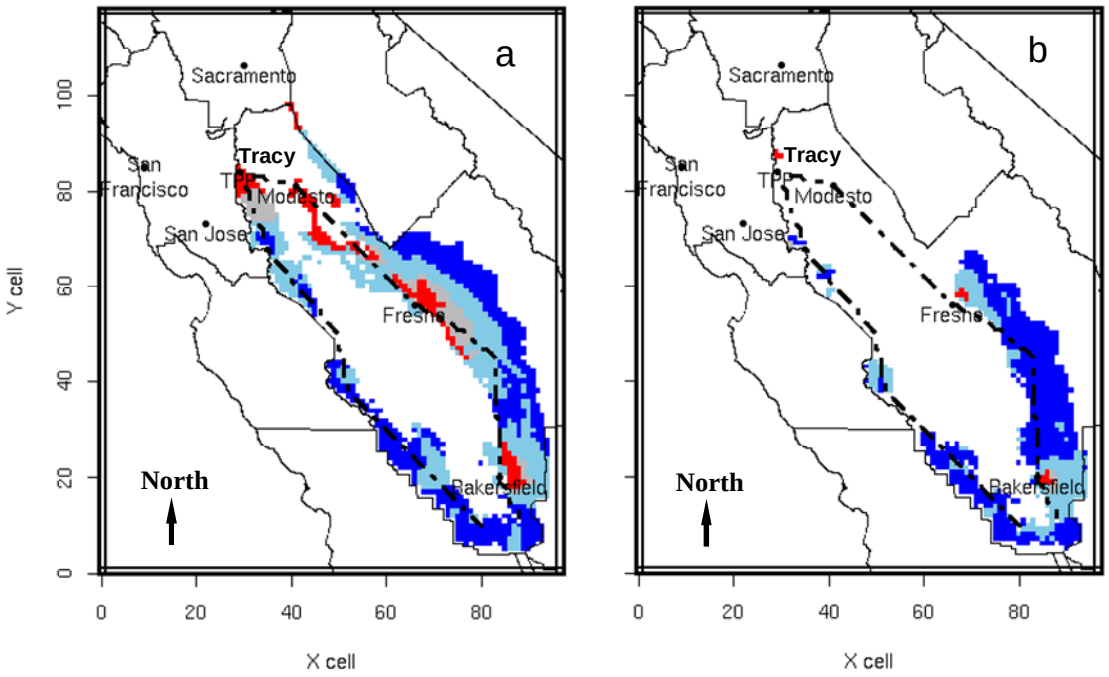

Figure 3. Mapping of ozone sensitivity options at 8-hr peak ozone exceedances in the SJV: **a**. weekdays, **b**: weekends. Locations always in "VOC control" are coded in red; NO_x control always beneficial ($\frac{\partial[O_3]}{\partial \varepsilon_{E_{NO_x}}} > 0$) in light blue, among which, the locations that are always in "NOx control" option ($\frac{\partial[O_3]}{\partial \varepsilon_{E_{NO_x}}} > \frac{\partial[O_3]}{\partial \varepsilon_{E_{AVOC}}}$) are further coded in blue; and finally, a mixed regime ($\frac{\partial[O_3]}{\partial \varepsilon_{E_{NO_x}}}$ changes signs) in grey. The non-exceedance areas in SJV are marked in white.

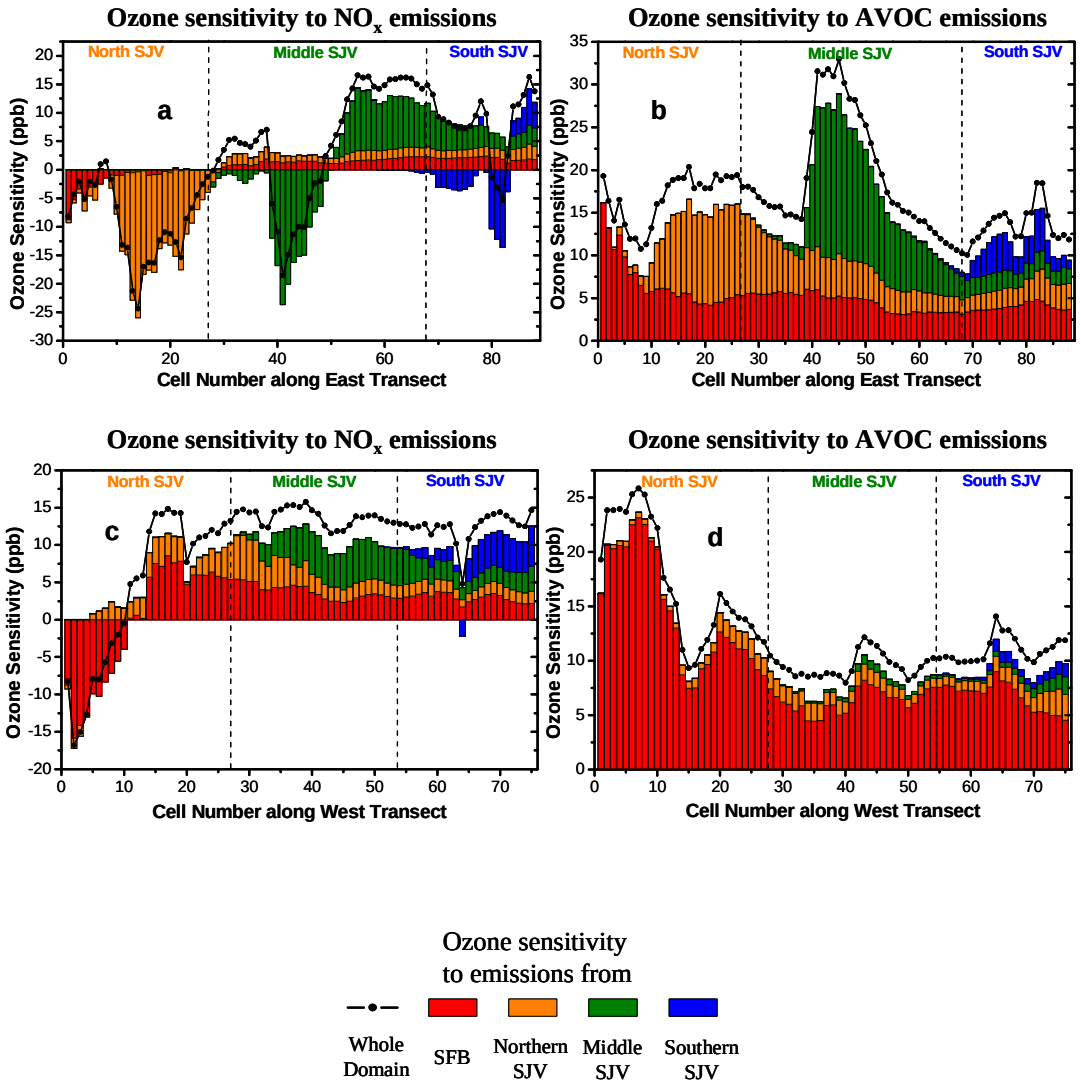

Figure 4. Weekday average 8-hr peak ozone sensitivities and decomposition of contributions from subregions: **a**. ozone sensitivity to NO_x emissions along the east transect; **b**. ozone sensitivity to AVOC emissions along the east transect; **c**. ozone sensitivity to NO_x emissions along the west transect; **d**. ozone sensitivity to AVOC emissions along the west transect. The transects run from north to south along the San Joaquin Valley, and are shown as dashed lines in Figure 3.

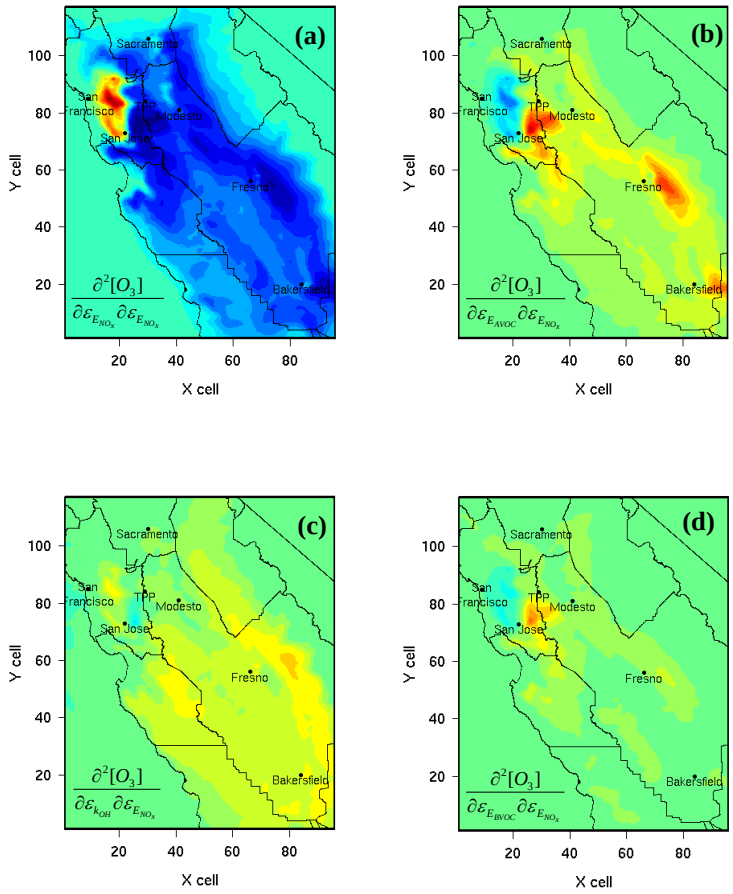

Figure 5. Weekday average second-order sensitivities of 8-hr peak ozone. These are sensitivities of $\frac{\partial[O_3]}{\partial\varepsilon_{E_{NO_x}}}$ to (a) NO_x emissions, (b) AVOC emissions, (c) $OH+NO_2$ rate coefficient, (d) BVOC emissions.